

# Streamwise and doubly-localised periodic orbits in plane Poiseuille flow

STEFAN ZAMMERT<sup>1</sup> † AND BRUNO ECKHARDT<sup>1,2</sup>

<sup>1</sup> Fachbereich Physik, Philipps-Universität Marburg, Renthof 6, D-35032 Marburg, Germany

<sup>2</sup> J.M. Burgerscentrum, Delft University of Technology, Mekelweg 2, 2628 CD Delft, The Netherlands

(Received 28 February 2022)

We study localised exact coherent structures in plane Poiseuille flow that are relative periodic orbits. They are obtained from extended states in smaller periodically continued domains, by increasing the length to obtain streamwise localisation and then by increasing the width to achieve spanwise localisation. The states maintain the travelling wave structure of the extended states, which is then modulated by a localised envelope on larger scales. In the streamwise direction, the envelope shows exponential localisation, with different exponents on the upstream and downstream sides. The upstream exponent increases linearly with Reynolds number  $Re$ , but the downstream exponent is essentially independent of  $Re$ . In the spanwise direction the decay is compatible with a power-law localisation. As the width increases the localised state undergoes further bifurcations which add additional unstable directions, so that the edge state, the relative attractor on the boundary between the laminar and turbulent motions, in the system becomes chaotic.

## 1. Introduction

The study of coherent structures in small periodic domains, often referred to as ‘minimal flow units’, has provided considerable insight into the phase-space structure and the transition dynamics of shear flows without linear instabilities of the laminar state, such as pipe flow or plane Couette flow and various boundary layers (e.g. Kreilos & Eckhardt (2012) and references therein). For an understanding of the fascinating spatio-temporal dynamics in the transition region, where intriguing patterns of alternating laminar and turbulent dynamics (Barkley & Tuckerman 2005; Duguet *et al.* 2010) and a complicated evolution that has been linked to directed percolation (Manneville 2009; Moxey & Barkley 2010; Avila *et al.* 2011) can be observed, it is necessary to investigate spatially extended domains and localised states. The interest in localised solutions also arises from the possibility of using them as building blocks for more complicated spatial patterns, such as the turbulent spots observed in plane Couette or plane Poiseuille flow in various experimental (e.g. Carlson *et al.* 1982; Dauchot & Daviaud 1995; Hegseth 1996; Lemoult *et al.* 2013) and numerical (e.g. Henningson *et al.* 1987; Lundbladh & Johansson 1991; Schumacher & Eckhardt 2001) studies.

The spatially extended exact coherent structures arise in the form of stationary states without any time-dependence, travelling waves where a pattern moves downstream with a fixed speed, or relative periodic orbits that return to the initial pattern except for a displacement (Nagata 1990, 1997; Ehrenstein *et al.* 1991; Schmiegél 1999; Wang *et al.* 2007; Gibson *et al.* 2009). Spanwise localised exact states have been identified by Schneider *et al.*

† Email address for correspondence: stefan.zammert@physik.uni-marburg.de

(2010*a,b*), Gibson & Brand (2014) and Zammert & Eckhardt (2014) for plane Couette and plane Poiseuille flow. Streamwise localised exact solutions have been described for the case of 2D plane Poiseuille flow (Price *et al.* 1993) and for pipe flow (Avila *et al.* 2013; Chantry *et al.* 2014). Spanwise localised states in plane Poiseuille flow show a complicated temporal dynamics (Zammert & Eckhardt 2014) that has also been documented for the asymptotic suction boundary layer by Khapko *et al.* (2013, 2014). A state in plane Couette flow that is localised in both the spanwise and streamwise directions has been identified recently by Brand & Gibson (2014).

In this paper we present coherent structures for plane Poiseuille flow that are localised in the streamwise direction and in streamwise and spanwise direction. We find them using the method of edge tracking (Skufca *et al.* 2006) in small periodic domains, and then continue them first to longer and then also to wider domains. We begin with a discussion of the extended states in narrow domains in section 2, followed by studies of streamwise localised states in section 3 and spanwise and streamwise localised structures in section 4. Conclusions are given in section 5.

## 2. The edge state in short domains - a traveling wave

We study the incompressible plane Poiseuille flow (PPF), the pressure driven flow between two infinitely extended parallel plates. With the  $x$ -axis along the flow direction, the plates are parallel to the  $x$ - $z$  plane at  $y = \pm h$ . The Reynolds number is based on  $h$ , the laminar centreline velocity  $U_0$  and the kinematic viscosity  $\nu$ , so that  $Re = U_0 h / \nu$  and the laminar non-dimensional profile becomes  $U(y) = (1 - y^2)$ . In all our simulations constant mass flux is imposed. The velocity fields used in the following are the deviations from the laminar profile, denoted  $\mathbf{u} = (u, v, w)$ , where  $u$ ,  $v$  and  $w$  are the streamwise, wall-normal and spanwise velocity components, respectively.

The numerical simulations are based on the spectral code *channelflow*, developed and maintained by Gibson (2012). The package provides a Newton method (Viswanath 2007) for searching for exact solutions as well as tools for continuation and stability analysis. We adapted the *channelflow*-code to work with parallel FFTW (OpenMP) and replaced the *Octave*-library used for the linear algebra routines in the Newton method and the eigenvalue calculations by the *Eigen*-package (Guennebaud, Jacon & Others 2010). The method of the edge tracking algorithm is described, e.g. by Toh & Itano (2003), Skufca *et al.* (2006), Schneider *et al.* (2008) and Dijkstra *et al.* (2014).

We started off with edge tracking from a random initial condition in a small periodic domain with streamwise length  $L_x$  of  $2\pi$  and spanwise width  $L_z$  of  $2\pi$  with a numerical resolution of  $N_x \times N_y \times N_z = 32 \times 65 \times 48$  and a Reynolds number of 1400. We checked our resolution by comparing to a higher one of  $N_x \times N_y \times N_z = 80 \times 97 \times 112$ . For this  $Re$  plane Poiseuille flow shows persistent turbulence although it is far below the critical Reynolds number of 5772 (Orszag 1971) that follows from linear stability theory. Note that on account of the domain length of  $2\pi$  the actual critical Reynolds number in this domain is 5815. Edge tracking usually converges quickly to one travelling wave, referred to as  $TW_E$  in the following. This state has two symmetries: a mirror symmetry with respect to the mid-plane, and a shift-and-reflect symmetry in the spanwise direction,

$$s_y : [u, v, w](x, y, z) = [u, -v, w](x, -y, z), \quad (2.1)$$

$$s_z \tau_x : [u, v, w](x, y, z) = [u, v, -w](x + L_x/2, y, -z). \quad (2.2)$$

The state is dominated by a strong low-speed streak in the mid-plane and pairs of vortices at the top and bottom plate. The travelling waves has the same symmetry as TW1-1 from Gibson & Brand (2014) and W01 from Waleffe (2001) and Nagata & Deguchi (2013).

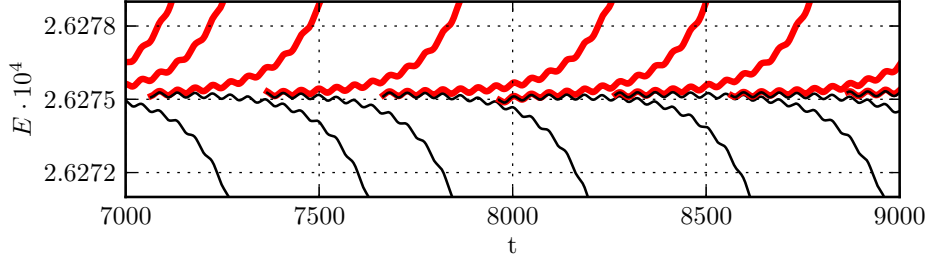


FIGURE 1. Edge tracking in a computational domain of length  $L_x = 32\pi$  and width  $L_z = 2\pi$  for  $Re = 1400$ . Shown are the energy densities of trajectories that turn turbulent (red thick) and laminar (black thin), respectively. The edge state bracketed by these trajectories oscillates periodically in energy.

Stability analysis of the travelling wave in the full space without any symmetry restriction shows that it has one unstable eigenvalue for  $510 < Re < 5850$  so that its stable manifold is of co-dimension one. A stability analysis of this periodic state in longer domains shows that for  $L_x = 4\pi$  the state already has an additional pair of unstable complex-conjugated eigenvalues for  $Re < 1785$ . Further doubling of the domain size adds more unstable directions, so that, e.g., for  $L_x = 8\pi$  and  $Re = 1400$  the wave has 5 unstable eigenvalues. The long-wavelength instabilities in the larger domains are precursors to localisation in the spanwise (Melnikov *et al.* 2014) and streamwise directions (Chantray *et al.* 2014).

### 3. Streamwise localised periodic orbits in long domains

In a longer domain of length  $32\pi$  but with the same width of  $2\pi$  and at Reynolds number  $Re = 1400$ , edge tracking converges to a state that at first glance looks like a state of constant energy density,

$$E(\mathbf{u}) = \frac{1}{4L_x L_z} \int \mathbf{u}^2 dx dy dz. \quad (3.1)$$

However, closer inspection of the time trace in figure 1 reveals that it is not constant but shows a regular oscillation with an amplitude of order  $10^{-8}$ . This oscillation is not a numerical artefact but reflects properties of the edge state, as we now show.

Although the initial velocity field is spatially non-localised, the flow state obtained by edge tracking is localised in the streamwise direction. Using this state as an initial condition in a Newton method, there is a quick convergence to a streamwise localised relative periodic orbit, referred to as  $PO_E$  in the following. For further study we transfer the state to a computational domain of length  $64\pi$ , which is possible because of its streamwise localisation. We use a resolution of  $768 \times 65 \times 48$  and check our results with a higher spanwise resolution of  $N_z = 80$ . The streamwise and the spanwise velocity components in the mid-plane are shown in figure 2. Cross-sections for  $Re = 1400$  for different streamwise positions are shown in figure 3 (a) - (d) and the streamwise averaged velocity is shown in (e). The images reveal that the orbit has a mirror symmetry ( $s_y$ ) but no  $s_z \tau_x$ -symmetry and is dominated by a strong narrow low-speed streak and a weak and extended high-speed streak. It is therefore very similar to the travelling wave  $TW_E$ . In particular, the streamwise-averaged flow for  $TW_E$  is close to the one shown in figure 3 (e).

The complex spatial propagation pattern of the wave can be seen in figure 4 where the

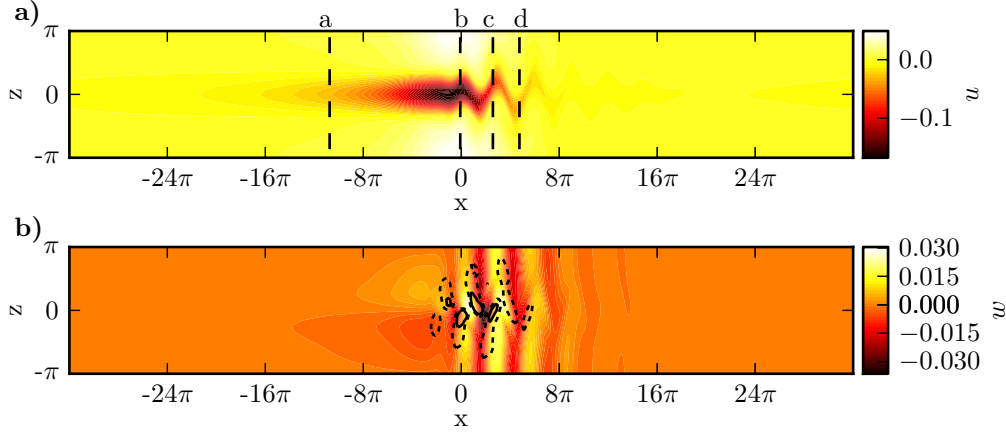


FIGURE 2. Instantaneous velocities in the mid-plane for the edge state  $PO_E$  at  $Re = 1400$  at the time of minimal energy. Shown are the (a) streamwise and (b) spanwise velocities. The black lines in (a) mark the positions of the spanwise wall-normal cross sections in 3 (a)-(d). The solid and dashed lines in (b) are iso-contours of the Q-vortex criterion (Jeong & Hussain 1995) at levels of  $0.001$  and  $0.0001$ , respectively. The direction of the flow is from left to right.

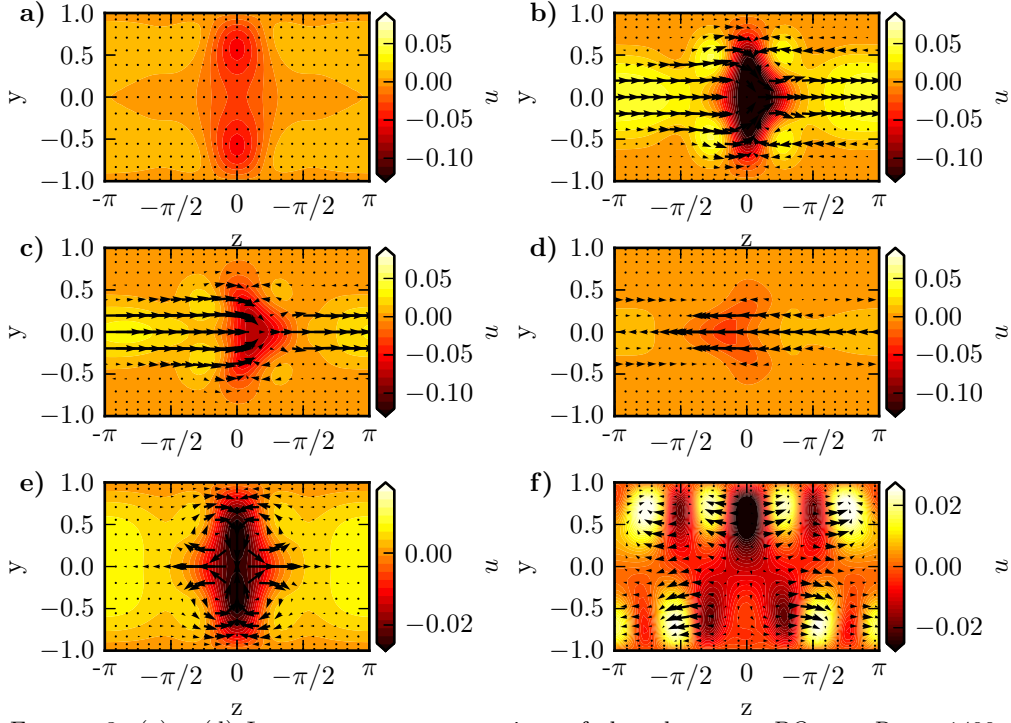


FIGURE 3. (a) - (d) Instantaneous cross sections of the edge state  $PO_E$  at  $Re = 1400$  at the streamwise positions indicated in figure 2(b). The in-plane components of the velocity are indicated by arrows and the streamwise component is colour coded. (e) and (f) show the streamwise-averages of  $PO_E$  at  $Re = 1400$  and of the orbit that bifurcates from it,  $PO_{asy}$ , at  $Re = 1625$ , respectively.

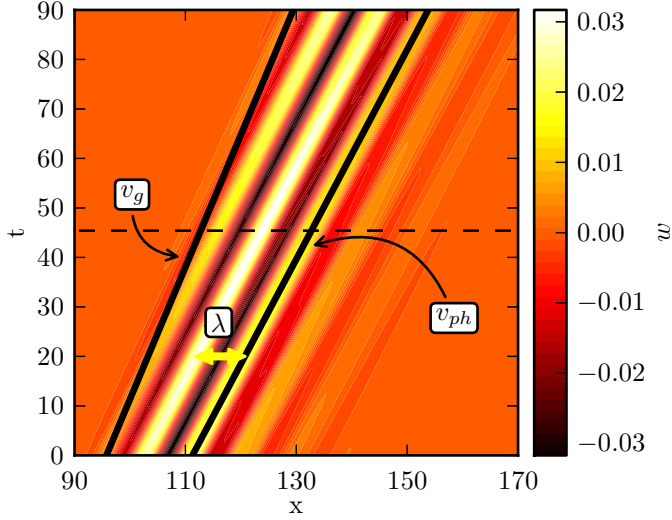


FIGURE 4. Space-time-display of the spanwise velocity of the periodic orbit  $PO_E$  in the mid-plane  $y = 0$  at  $z = 0$  for  $Re = 1400$ . The solid black lines indicate the group velocity  $v_g$  and the phase velocity  $v_{ph}$  for one of the maxima. The wavelength  $\lambda$  of the internal modulations varies along the state. The dashed black line marks one period  $T$  in energy.

spanwise velocity in the mid-plane at  $z = 0$  is plotted versus time for  $Re = 1400$ . The total energy of the state is periodic with a period  $T = 45.402$ , but the state needs twice this time to return in shape, apart from a downstream shift. After a time  $T$  it returns apart from a symmetry operation  $s_z : [u, v, w](x, y, z) = [u, v, -w](x, y, -z)$  and a downstream shift that is half the one after  $2T$ . The figure clearly shows a group velocity  $v_g$  for the envelope of the state, and a phase velocity  $v_{ph}$  for the underlying structures. The group velocity  $v_g$  can be calculated by dividing the distance travelled over two periods by  $2T$ . For  $Re = 1400$  one obtains  $v_g = 0.8753$ , indicated by the line at the upstream end of the state in figure 4. The structures underneath the envelope move with a different velocity  $v_{ph}$ , which can be read off from the slope of the maxima. However, the wavelength  $\lambda$  of the spanwise modulations varies slightly with position and is slightly larger at the front than in the centre and towards the end of the state. Therefore, the velocity of each maximum also varies slightly, so that the phase velocity depends on the position within the state.

Using a continuation method (see e.g. Dijkstra *et al.* 2014) it is easy to track the state in  $Re$ . It turns out that the periodic orbit exists down to  $Re \approx 1038$ , where it is created in a saddle-node bifurcation. Furthermore, it is also possible to identify the upper branch of the periodic orbit. This upper branch is also localised and has multiple unstable directions.

A stability analysis of the lower branch state shows that for  $Re > 1100$  it has one unstable direction. Therefore, for these Reynolds numbers the state is an edge state whose stable manifold can separate the state space into two parts. For lower values of  $Re$  the periodic orbit has more than one unstable direction. The bifurcation near  $Re \approx 1100$  is a Sacker-Neimark bifurcation (Kuznetsov 1998) that breaks the  $s_y$  symmetry. This bifurcation is followed by further bifurcations resulting in eight unstable directions for the lower branch. One of the bifurcations of the lower branch is a pitchfork bifurcation that breaks the  $s_y$  symmetry and creates an asymmetric periodic orbit ( $PO_{asy}$ ). The

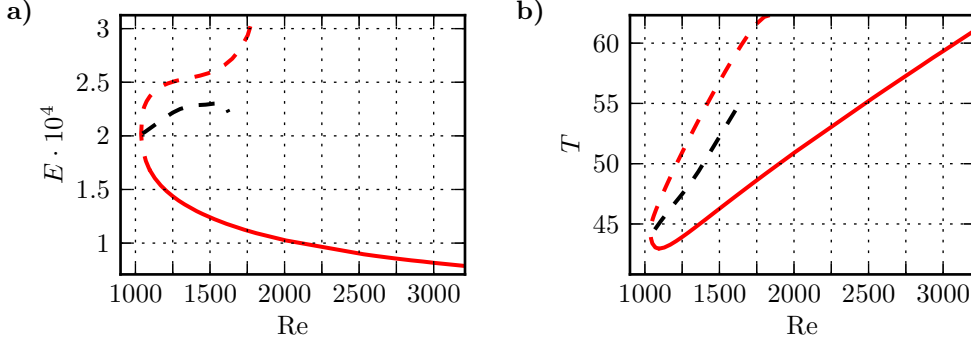


FIGURE 5. Bifurcation diagram for the coherent structures. (a) Minimum energy of the localised periodic orbit  $PO_E$  (red) and the asymmetric orbit  $PO_{asy}$  (black) vs  $Re$ . In both cases the minimum in energy over the period  $T$  is shown. The stability of the orbit is indicated by the linetype, solid for a single unstable direction, and dashed for more than one. (b) Variation of the periods in energy with  $Re$ .

image of the state in figure 3 (f) shows that its internal dynamics is more complex than that of  $PO_E$ . The bifurcations and some properties of the states are summarised in figure 5.

Information about the localisation properties can be extracted from the streamwise variation of the energy density of the deviation from the laminar flow,

$$E_{\perp}(x) = \frac{1}{4L_z} \int_0^{L_z} \int_{-1}^1 \mathbf{u}^2 \, dydz, \quad (3.2)$$

and the density of the cross-flow energy

$$E_{\perp,c}(x) = \frac{1}{4L_z} \int_0^{L_z} \int_{-1}^1 v^2 + w^2 \, dydz. \quad (3.3)$$

The energy densities for the periodic orbit at  $Re = 2010$  (at times of minimal energy) are shown in figure 6(a). One can identify a small region with relatively high cross-flow energy at the front of the state. In this region the cross-flow draws energy from the laminar profile and transfers it into streamwise velocity, which then drives streaks and causes a steep increase of the total energy density at the front of the state. The energy in the streamwise components has its maximum at a position in the tail where the cross-flow energy is already very low again. In the absence of cross-flow motion the streaks are damped by viscosity only, which results in the long tail of the state.

Based on the energy density  $E_{\perp}(x)$  one can introduce two characteristic length scales for  $PO_E$ , associated with the extension in the downstream and upstream direction. Starting from the maximum in energy, one can determine the distances to the locations where the energy density has dropped to half its maximum. They are denoted  $l_t$  and  $l_h$  for the upstream (tail) and downstream (head) sides, respectively, and are shown in figure 6(b). On the downstream side, the energy drops off quickly, on a length scale that varies very little with  $Re$ . On the upstream side, the energy drops off more slowly, on a length scale that increases linearly with  $Re$ . The origin of this scaling is the viscous decay of the streaks on a time scale proportional to  $Re$ , which then is translated into a spatial scale proportional to  $Re$  by the essentially constant advection velocity. In the case of plane Couette flow, Brand & Gibson (2014) have been able to determine the slopes from a linear stability analysis that confirms this scaling. The case of plane Poiseuille flow is

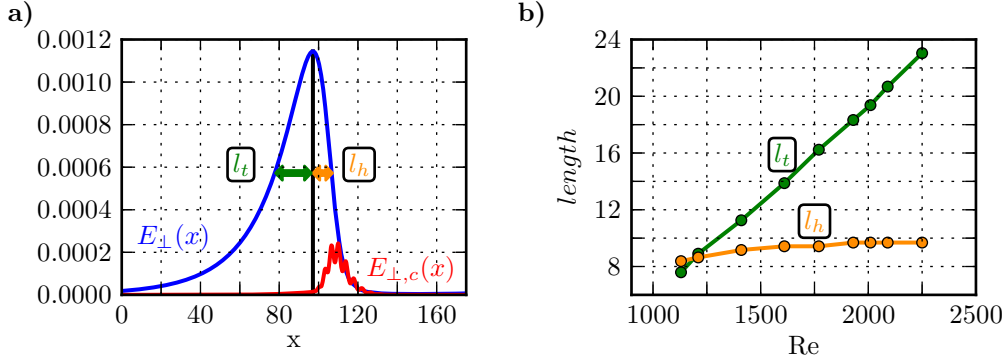


FIGURE 6. Energy profiles of the localised state. (a) Densities of total (red) and the cross flow (blue) energy for the periodic orbit at  $Re = 2010$  along the flow direction, which is from left to right. The cross flow energy density is multiplied by a factor of 10. (b) Downstream  $l_h$  (orange) and upstream  $l_t$  (green) distances from the maximum to half the maximal values in energy.

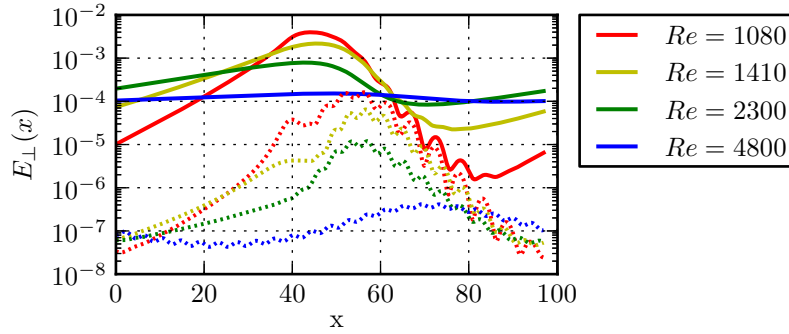


FIGURE 7. Profiles of  $PO_E$  for increasing Reynolds numbers. The solid lines show the total and the dashed lines the cross-flow energy densities. Consistent with the increase in  $l_d$ , the states become more and more delocalised with increasing Reynolds number, until they merge into a spatially extended state near  $Re = 5385$ . The streamwise length of the computational domain is  $32\pi$ .

more complicated because the state is not stationary, and an analytical calculation of the decay rates has not been possible, yet.

Although the structure becomes longer with increasing  $Re$ , the total energy and also the maximum of the energy density decrease with increasing  $Re$  (see figure 5). In finite domains the increasing length of the structures will then cause interference between head and tail and a loss of localisation. For instance, continuation of  $PO_E$  to high  $Re$  in a box of length  $32\pi$  shows that the orbit connects to the streamwise extended travelling wave  $TW_E$  at  $Re \approx 5385$  with a wavelength of  $2.66\pi$ . This is documented in figure 7 in a plot of the energy densities vs.  $Re$ . For low  $Re$  there is a pronounced maximum in the densities, but for increasing  $Re$  the differences decrease and finally at  $Re \approx 5380$  the uniform energy density corresponding to the travelling wave is obtained. Turned the other way round, the localised state arises out of a streamwise long-wavelength instability of a travelling wave, very much like the long wavelength instabilities discussed in plane Couette flow (Melnikov *et al.* 2014) or in pipe flow (Chantry *et al.* 2014).

#### 4. A streamwise and spanwise localised periodic orbit

The periodic orbits found in the domain with  $L_z = 2\pi$  are localised in the streamwise direction. They show early signs of localisation in the spanwise direction in that the energy density close to the strong low-speed streak is much higher than in the region of the high-speed streak. To obtain periodic orbits that are also localised in the spanwise direction we continue the periodic orbit in box width. For the continuation in  $L_z$  we fix  $Re = 2180$  and a length of  $64\pi$ . As a measure of the state we consider the energy density obtained by averaging over the streamwise and normal directions,

$$E_{\parallel}(z) = \frac{1}{4L_x} \int_0^{L_x} \int_{-1}^1 \mathbf{u}^2 \, dx dy. \quad (4.1)$$

This partially averaged energy density depends on the spanwise coordinate only, and is shown in figure 8(a) for various widths  $L_z$ . The maximum at  $z = 0$  corresponds to the position of the low-speed streak. For  $L_z = 2\pi$  the second smaller maximum is the position of the weak high-speed streak. Slightly above  $L_z = 2\pi$  the lower maximum splits into two. For  $L_z > 5\pi$  the energy density has a very low value over most of the domain, indicating a spanwise localised flow structure. The largest value of  $L_z$  which we studied is  $72\pi$ . For this domain we use a resolution of  $N_x \times N_y \times N_z = 384 \times 49 \times 1728$ . The doubly-localised solution in this domain keeps the  $s_y$  symmetry of the state that is localised in the streamwise direction only. The period  $T$  of the orbit is 53.578. After this time the state returns in shape up to a downstream shift and the symmetry operation  $s_z$ . The group speed of the orbit is  $v_g = 0.8803$ .

The logarithmic scale in figure 8(a) shows that  $E_{\parallel}(z)$  does not drop off exponentially in the spanwise direction. Since the integrated density increases with the length of the turbulent region, a much better measure is the maximum in velocities along  $x$  and  $y$  for a fixed spanwise position, i.e the  $\infty$ -norm  $\mathcal{L}^{\infty}(u) = \max_{x,y} |u(x, y, z)|$ , here given for the streamwise component  $u$  (Brand & Gibson 2014). Its values for the streamwise and spanwise component are shown in figure 9(a). The decay of  $\mathcal{L}^{\infty}(u)$  is slower than exponential while  $\mathcal{L}^{\infty}(w)$  drops off faster. The second part is hidden in  $E_{\parallel}(z)$  because it is swamped by the higher values of the streamwise component. The behaviour near  $z = L_z$  is clearly influenced by the boundary conditions: the streamwise component is symmetric under reflection at the boundary, whereas the spanwise component is antisymmetric and vanishes at the boundary. Taking this into account, the figure also shows fits to an algebraic decay with the correct symmetries: the agreement between the fit and the numerical data indicates that the velocity fields fall off like  $1/z^2$  over the width of the domain.

In the streamwise direction, as documented in figure 9(b), the decay is exponential for the domain sizes studied here. This agrees with the observations on the partially localised states in section 3, including the asymmetry in the decays in the upstream and downstream direction.

Images of the streamwise and the spanwise velocity fields in the mid-plane are shown in figure 10. The visualisation of the spanwise velocity reveals a large-scale, quadrupolar-like flow field, where the centres of the left and the right pairs of lobes coincide with intensity maxima of  $E_{\perp,c}(x)$ . The quadrupolar shape of the spanwise velocity also exists away from the mid-plane, but becomes less distinct close to the walls. Given the observation of similar large scale quadrupole flows in turbulent spots in plane Couette (e.g. Schumacher & Eckhardt 2001; Lagha & Manneville 2007; Duguet & Schlatter 2013; Gibson & Brand 2014) and plane Poiseuille flow (Lemoult *et al.* 2013, 2014), one can anticipate that they appear for all structures that are localised in all directions.



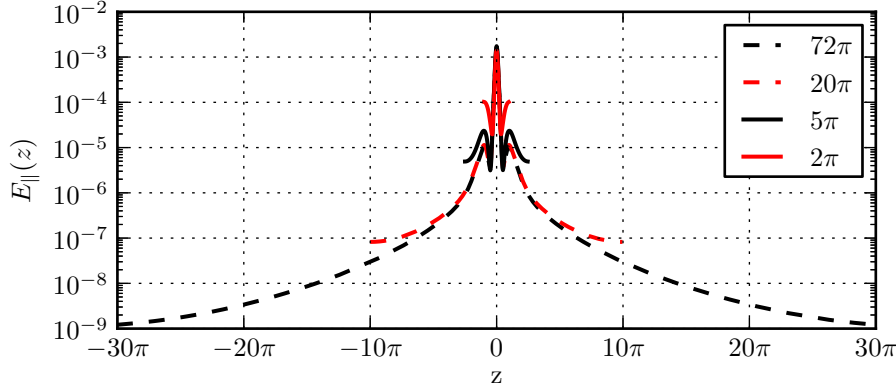


FIGURE 8. Spanwise profiles of the total energy of the localised states  $PO_E$  for various spanwise widths  $L_z$ .

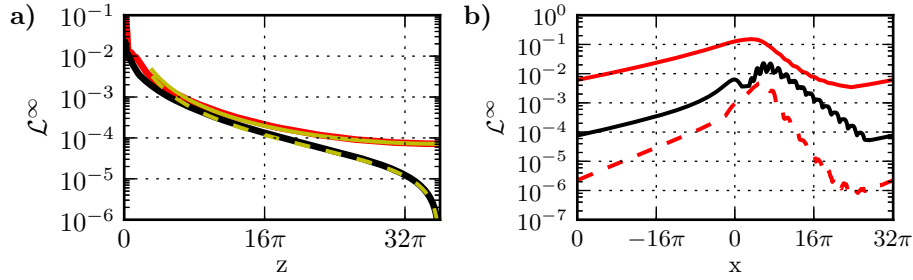


FIGURE 9. In (a) the  $\mathcal{L}^\infty$ -norm (maximum over  $y$  and  $x$ ) of the streamwise  $u$  (solid red), the spanwise  $w$  (solid black) velocity component versus spanwise coordinate  $z$  are shown. The yellow lines show fits  $A(z^{-2} + (L_z - z)^{-2})$  (solid) and  $A(z^{-2} - (L_z - z)^{-2})$  (dashed). (b) shows the  $\mathcal{L}^\infty$ -norms (maximum over  $y$  and  $z$ ) of the streamwise (solid red), spanwise (black) and wall-normal (dashed red) velocity component versus streamwise coordinate  $x$ .

We verified that we can trace the doubly-localised solution in the domain with  $L_x = 64\pi$  and  $L_z = 72\pi$  also to lower and higher values of  $Re$ , but because applying the Newton method to this large domain is computationally very expensive, we did not perform a complete continuation in Reynolds number.

A stability analysis of the localised state as a function of  $L_z$  at  $Re = 2180$  shows that it has two unstable eigenvalues for  $L_z \geq 6\pi$ . Therefore, it is not an attracting state at the laminar-turbulent boundary. Edge tracking calculations starting from the disturbed localised periodic orbit do not result in a simple attractor. Instead, the time evolution of the state is chaotic, but it remains localised (Zammert & Eckhardt 2014b). This behaviour is similar to what has been seen in large plane Couette domains (Marinc *et al.* 2010; Schneider *et al.* 2010b; Duguet *et al.* 2009), long pipes (Mellibovsky *et al.* 2009), or wide domains in the asymptotic suction boundary layer (Khapko *et al.* 2014).

## 5. Conclusions and Outlook

We were able to identify a doubly-localised periodic orbit in plane Poiseuille flow. The orbit was shown to bifurcate from a streamwise extended travelling wave. Together with the other current examples of long-wavelength instabilities (Melnikov *et al.* 2014;

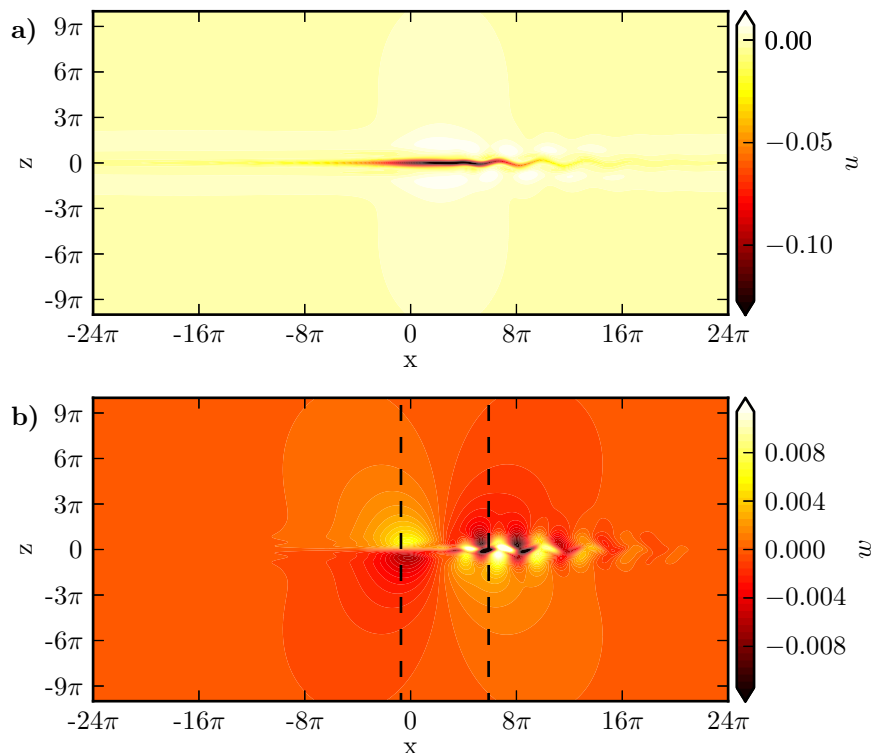


FIGURE 10. Instantaneous streamwise (a) and spanwise (b) velocity in the mid-plane for the doubly-localised periodic orbit at  $Re = 2180$  in a domain with  $L_x = 64\pi$  and  $L_z = 72\pi$ . The snapshot is for the time of minimal energy during one period. Only the part of the domain that contains the localised flow structure is shown. The dashed lines in (b) mark the downstream positions of the maxima in the energy density  $E_{\perp,c}(x)$ .

Chantry *et al.* 2014) we anticipate that many more localised states can be found in bifurcations of the of spatially extended states that have been identified already (Schmiegel 1999; Gibson *et al.* 2009). Homotopies between plane Poiseuille flow and other flows, including plane Couette or the asymptotic suction boundary layer, can then reveal connections between these states (Waleffe 2003; Kreilos *et al.* 2013). More generally, the presence of localised states opens up the path to spatial delocalisation and the development of spatio-temporal patterns (see e.g. Barkley & Tuckerman 2005; Avila *et al.* 2011; Tuckerman *et al.* 2014).

**Acknowledgements** We thank John Gibson for providing *channelflow* and stimulating exchanges on localisation properties. We also thank Yohann Duguet and Tobias Kreilos for discussions. This work was supported by the Deutsche Forschungsgemeinschaft within FOR 1182.

#### REFERENCES

- AVILA, K., MOXEY, D., DE LOZAR, A., AVILA, M., BARKLEY, D. & HOF, B. 2011 The onset of turbulence in pipe flow. *Science* **333** (6039), 192–196.
- AVILA, M., MELLIBOVSKY, F., ROLAND, N. & HOF, B. 2013 Streamwise-localised solutions at the onset of turbulence in pipe flow. *Phys. Rev. Lett.* **110**, 224502.

- BARKLEY, D. & TUCKERMAN, L. 2005 Computational study of turbulent laminar patterns in Couette flow. *Phys. Rev. Lett.* **94**, 014502.
- BRAND, E. & GIBSON, J.F. 2014 A doubly-localised equilibrium solution of plane Couette flow. *J. Fluid Mech.* **750**, R1.
- CARLSON, D. R., WIDNALL, S. E. & PEETERS, M. F. 1982 A flow-visualization study of transition in plane Poiseuille flow. *J. Fluid Mech.* **121**, 487–505.
- CHANTRY, M., WILLIS, A. P. & KERSWELL, R. R. 2013 The genesis of streamwise-localised solutions from globally periodic travelling waves in pipe flow. *Phys. Rev. Lett.* **112**, 164501.
- DAUCHOT, O. & DAVIAUD, F. 1995 Finite amplitude perturbation and spots growth mechanism in plane Couette flow. *Phys. Fluids* **7**, 335.
- DIJKSTRA, H., *et al.* 2014 Numerical bifurcation methods and their application to fluid dynamics: Analysis beyond simulation. *Commun. Comput. Phys.* **15**, 1–45.
- DUGUET, Y. & SCHLATTER, P. 2013 Oblique laminar-turbulent interfaces in plane shear flows. *Phys. Rev. Lett.* **110**, 034502.
- DUGUET, Y., SCHLATTER, P. & HENNINGSON, D. S. 2009 Localised edge states in plane Couette flow. *Phys. Fluids* **21**, 111701.
- DUGUET, Y., SCHLATTER, P. & HENNINGSON, D. S. 2010 Formation of turbulent patterns near the onset of transition in plane Couette flow. *J. Fluid Mech.* **228**, 119–129.
- EHRENSTEIN, U. & KOCH, W. 1991 Three-dimensional wavelike equilibrium states in plane Poiseuille flow. *J. Fluid Mech.* **121**, 111–148.
- GIBSON, J. F. 2012 Channelflow: A spectral Navier-Stokes simulator in C++. *Tech. Rep.*. U. New Hampshire.
- GIBSON, J. F. & BRAND, E. 2014 Spanwise-localised solutions of planar shear flows. *J. Fluid Mech.* **745**, 25–61.
- GIBSON, J. F., HALCROW, J. & CVITANOVIĆ, P. 2009 Equilibrium and travelling-wave solutions of plane Couette flow. *J. Fluid Mech.* **638**, 243–266.
- GUENNEBAUD, G., JACON, B. & OTHERS 2010 Eigen v3.
- HEGSETH, J. 1996 Turbulent spots in plane Couette flow. *Phys. Rev. E* **54**, 4915–4923.
- HENNINGSON, D., SPALART, P. & KIM, J. 1987 Numerical simulations of turbulent spots in plane Poiseuille and boundary-layer flow. *Phys. Fluids* **30**, 2914.
- JEONG, J. & HUSSAIN, F. 1995 On the identification of a vortex. *J. Fluid Mech.* **285**, 69–94.
- KHAPKO, T., KREILOS, T., SCHLATTER, P., DUGUET, Y., ECKHARDT, B. & HENNINGSON, D. S. 2013 Localised edge states in the asymptotic suction boundary layer. *J. Fluid Mech.* **717**, R6.
- KHAPKO, T., DUGUET, Y., KREILOS, T., SCHLATTER, P., ECKHARDT, B. & HENNINGSON, D. S. 2014 Complexity of localised coherent structures in a boundary-layer flow. *Eur. Phys. J. E* **37**, 32.
- KREILOS, T. & ECKHARDT, B. 2012 Periodic orbits near onset of chaos in plane Couette flow. *Chaos* **22**, 047505.
- KREILOS, T., VEBLE, G., SCHNEIDER, T. M. & ECKHARDT, B. 2013 Edge states for the turbulence transition in the asymptotic suction boundary layer. *J. Fluid Mech.* **726**, 100–122.
- KUZNETSOV, Y.A. 1998 *Elements of applied bifurcation theory*. Springer Berlin / Heidelberg.
- LAGHA, M. & MANNEVILLE, P. 2007 Modeling of plane Couette flow. I. Large scale flow around turbulent spots. *Phys. Fluids* **19**, 094105.
- LEMOULT, G., AIDER, J.-L. & WESFREID, J. E. 2013a Turbulent spots in a channel: large-scale flow and self-sustainability. *J. Fluid Mech.* **731**, R1.
- LEMOULT, G., GUMOWSKI, K., AIDER, J.-L. & WESFREID, J. E. 2014 Turbulent spots in channel : an experimental study Large-scale flow, inner structure and low order model. *Eur. Phys. J. E* **37**, 25.
- LUNDBLADH, A. & JOHANSSON, A. V. 1991 Direct simulation of turbulent spots in plane Couette flow. *J. Fluid Mech.* **229**.
- MANNEVILLE, P. 2009 Spatiotemporal perspective on the decay of turbulence in wall-bounded flows. *Phys. Rev. E* **79**, 025301.
- MARINC, D., SCHNEIDER, T. M. & ECKHARDT, B. 2010 localised edge states for the transition to turbulence in shear flows. In *Seventh IUTAM Symp. Laminar-Turbulent Transit.* (ed. Philipp Schlatter & Dan S. Henningson), *IUTAM Bookseries*, vol. 18, pp. 253–258. Dordrecht: Springer Netherlands.

- MELLIBOVSKY, F., MESEGUER, A., SCHNEIDER, T. & ECKHARDT, B. 2009 Transition in localised Pipe Flow Turbulence. *Phys. Rev. Lett.* **103**, 054502.
- MELNIKOV, K., KREILOS, T. & ECKHARDT, B. 2014 Long wavelength instability of coherent structures in plane Couette flow. *Phys. Rev. E* **89**, 043088.
- MOXEY, D. & BARKLEY, D. 2010 Distinct large-scale turbulent-laminar states in transitional pipe flow. *Proc. Natl. Acad. Sci. U. S. A.* **107**, 8091–8096.
- NAGATA, M. 1990 Three-dimensional finite-amplitude solutions in plane Couette flow: bifurcation from infinity. *J. Fluid Mech.* **217**, 519–527.
- NAGATA, M. 1997 Three-dimensional traveling-wave solutions in plane Couette flow. *Phys. Rev. E* **55**, 2023–2025.
- NAGATA, M. & DEGUCHI, K. 2013 Mirror-symmetric exact coherent states in plane Poiseuille flow. *J. Fluid Mech.* **735**, R4.
- ORSZAG, S. A. 1971 Accurate solution of the Orr–Sommerfeld stability equation. *J. Fluid Mech.* **50**, 689–703.
- PRICE, T., BRACHET, M. & POMEAU, Y. 1993 Numerical characterization of localised solutions in plane Poiseuille flow. *Phys. Fluids A Fluid Dyn.* **5**, 762.
- SCHMIEGEL, ARMIN 1999 Transition to turbulence in linearly stable shear flows. Phd thesis, Marburg.
- SCHNEIDER, T. M., GIBSON, J. F., LAGHA, M., DE LILLO, F. & ECKHARDT, B. 2008 Laminar-turbulent boundary in plane Couette flow. *Phys. Rev. E* **78**, 037301.
- SCHNEIDER, T. M., GIBSON, J. F. & BURKE, J. 2010a Snakes and ladders: Localised solutions of plane Couette flow. *Phys. Rev. Lett.* **104**, 104501.
- SCHNEIDER, T. M., MARINC, D. & ECKHARDT, B. 2010b localised edge states nucleate turbulence in extended plane Couette cells. *J. Fluid Mech.* **646**, 441.
- SCHUMACHER, J. & ECKHARDT, B. 2001 Evolution of turbulent spots in a parallel shear flow. *Phys. Rev. E* **63**, 046307.
- SKUFCA, J., YORKE, J. & ECKHARDT, B. 2006 Edge of chaos in a parallel shear flow. *Phys. Rev. Lett.* **96**, 174101.
- TOH, S. & ITANO, T. 2003 A periodic-like solution in channel flow. *J. Fluid Mech.* **481**, 67–76.
- TUCKERMAN, L., KREILOS, T., SCHROBSDORFF, H., SCHNEIDER, T.M. & GIBSON, J. F. 2014 Turbulent-laminar patterns in plane Poiseuille flow. *arXiv1312.6783*
- VISWANATH, D. 2007 Recurrent motions within plane Couette turbulence. *J. Fluid Mech.* **580**, 339.
- WALEFFE, F. 2001 Exact coherent structures in channel flow. *J. Fluid Mech.* **435**, 93–102.
- WALEFFE, F. 2003 Homotopy of exact coherent structures in plane shear flows. *Phys. Fluids* **15**, 1517.
- WANG, J., GIBSON, J. F. & WALEFFE, F. 2007 Lower branch coherent states in shear flows: Transition and control. *Phys. Rev. Lett.* **98**, 204501.
- ZAMMERT, S. & ECKHARDT, B. 2014 Periodically bursting edge states in plane Poiseuille flow. *Fluid. Dyn. Res.* **46**, 041419.
- ZAMMERT, S. & ECKHARDT, B. 2014b A spotlike edge state in plane Poiseuille flow. *Proc. Appl. Math. Mech.* submitted.